Experimental investigations of supersonic turbulent flow over a compression ramp

Wu Yu, Yi Shihe, He Lin*, Chen Zhi and Zhu Yangzhu

National University of Defense Technology, Changsha 410073, China

Experimental studies of supersonic flow over a 28° compression ramp were carried out in a Mach 3.0 wind tunnel; the incoming boundary layer was turbulent flow. Fine flow structures were visualized via NPLS (nano-tracer-based planar laser scattering) technique. Analysis of two NPLS images between 10 μs revealed the spatio-temporal evolutions of flow field. The angles of separation shock and reattachment shock, and the development of boundary layer after reattachment were measured by time-averaged flow field. Velocity field structures were measured using particle image velocimetry technique. Streamlines in the mean velocity field indicated reverse flow in separation region, and variations of velocity vectors showed velocity shear. Moreover, flow separation and reattachment were clearly revealed by the analysis of velocity field.

Keywords: Compression ramp, nano-tracer, turbulent flow, velocity field.

AS a typical geometric configuration, compression ramp can be widely seen on the surface of aircraft. In supersonic flow, the separated flow and shock wave boundary-layer interactions which are caused by compression ramp make the flow field complicated, and have a major influence on flow structures. As a classical compressible turbulent flow, it is important in academic research and engineering application. In the past several decades, several numerical simulations and experimental studies have been carried out, focusing on flow structures, wall pressure, heat flux and velocity field. Wu and Martin[1] used direct numerical simulation (DNS) data of a Mach 2.9, 24° compression ramp flow to analyse the features of upstream boundary layer and wall pressure, the physical dimension of separation bubble and the downstream velocity profile. The shock motion had been observed by wall pressure and mass flux signals measured in free stream. Edwards *et al.*[2] used a hybrid large-eddy/Reynolds-averaged Navier–Stokes model to perform simulations of Mach 5 turbulent flow over a 28° compression corner. Compared with Reynolds-averaged model, this model predicted more amplification of the Reynolds stresses probably due to reattachment shock motion. Dawson *et al.*[3] analysed the low-frequency motion of shock and separation bubble through large-eddy simulation (LES) of Mach 2.9 turbulent boundary layer over a 24° compression ramp. Their results indicated a strong connection between the motion of shock and size of the separation bubble; fluctuations of streamwise velocity were maximum in the shear layer.

Gramann and Dolling[4] studied turbulent structures associated with separation shock motion of Mach 5, 28° compression ramp. Measurements of fluctuating wall and pitot pressure were simultaneously sampled at locations of 20 boundary layer thickness upstream of the ramp. The data showed that the separation bubble whose streamwise length varied from 1.7 to 3.6 boundary layer thickness expanded and contracted at the same frequencies as the separation shock motion. Ringuette and Bookey[5] conducted experiments to study the turbulent interaction in a Mach 2.9 compression ramp. The flow structures were visualized by filtered Rayleigh scattering (FRS) and some quantitative measurements such as the turbulent structure angle, the length of separation bubble and the intermittency of boundary layer were provided. Chan *et al.*[6] revealed details of the incoming boundary layer and the separation shock through pressure measurements and planar laser mie scattering (PLMS) in a Mach 5 28° compression ramp flow. Analysis of flow visualization data suggested that the incoming boundary layer was comprised of large-scale structures containing streamwise components of vorticity, and the low frequency motion of separation shock was related to a thickening and thinning of the incoming boundary layer. Zheltovodov[7] reviewed some recent experimental and computational methods in 2D and 3D compression ramp. He also proposed some perspectives and problems for future studies.

Although the aforementioned studies referred to many aspects of compression ramp, the previous experiment data had low resolution on flow structures. Traditional flow visualization techniques such as schlieren and shadow exhibit low spatial resolution, while PLMS and FRS encounter weak scattering signals and low signal-to-noise ratio. As a result, it is difficult to achieve the measuring requirements in supersonic flow using these techniques. Nano-tracer-based planar laser scattering (NPLS)[8,9] is a flow visualization technique for measuring fine structures in supersonic/hypersonic flow. Its spatial resolution is in the micrometre scale, with a time resolution of 6 ns; the temporal correlation resolution can reach 0.2 μs. In the present study, NPLS is applied to reveal the fine flow structures of a 28° compression ramp with turbulent upstream boundary layer; velocity field structures are obtained via PIV technique. The mean flow structures and spatio-temporal evolution of flow field are discussed here, and the characteristics of velocity field are analysed.

Experimental studies were carried out in a Mach 3 wind tunnel. To eliminate disturbances to the testing area, the wind tunnel was directly connected, and there were no rhombus regions at the outlet of the nozzle. The nozzle which ran in an indraft mode was designed based on a B-spline curve. The incoming flow was dried and

---

*For correspondence. (e-mail: helin.101sys@gmail.com)

dust-free, and the total pressure and stagnation temperature were $P_0 = 0.1$ MPa and $T_0 = 300$ K respectively; the unit Reynolds number was $\mathrm{Re} = 7.5 \times 10^6$/m. The diffuser was connected to vacuum downstream. The cross-section of the test chamber was 100 mm × 120 mm. The two side faces whose dimensions are 250 mm × 120 mm were installed with optical glass for measuring and imaging.

The experimental model of the compression ramp is shown in Figure 1. The length of forepart flat $l = 120$ mm, the length of ramp $s = 60$ mm, the spanwise width $d = 100$ mm, the ramp angle is 28° and the distance between the ceiling of the test chamber and the surface of the forepart flat $h = 120$ mm. Owing to the location of the model, the upstream boundary layer is turbulent flow which is fully developed along the wind tunnel wall. The spanwise width of the model is same as the spanwise size of the test chamber, which enables the flow to be considered as two-dimensional. It can be seen from Figure 1 that the theoretical angle of Mach wave induced by the fixing step is 20°, and the Mach wave does not disturb the testing region.

NPLS which is based on traditional planar laser scattering is a visualization technique for measuring fine flow structures using nanoparticles for tracing. With excellent following ability of nanoparticles, the distribution of the scattering light can reveal flow structures exactly. Therefore, NPLS is appropriate for measurements in high speed and complicated flow field. As shown in Figure 2, the NPLS system is composed of a light source, synchronous controller, imaging, data acquisition and processing systems as well as nanoparticles generator. A dual-cavity Nd : YAG pulsed laser which emits two laser beams of 532 nm wavelength and 6 ns pulse width is used as the light source. A light sheet less than 1 mm thick illuminates the regions of interest through the optical path and the lens. An interline transfer double-exposure CCD camera with resolution $2k \times 2k$ and a shortest double-exposure interval of 0.2 μs is used for taking images. The synchronizer, which has an accuracy of 250 ps, enables both the laser source and CCD camera to work simultaneously. The computer transmits instructions, and is also used for gathering, storing and processing images. Further details about the NPLS system can be found in the literature[9–13].

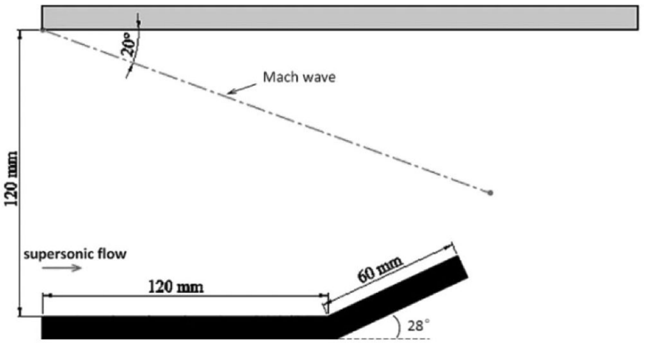

Figure 1. Sketch of compression ramp model.

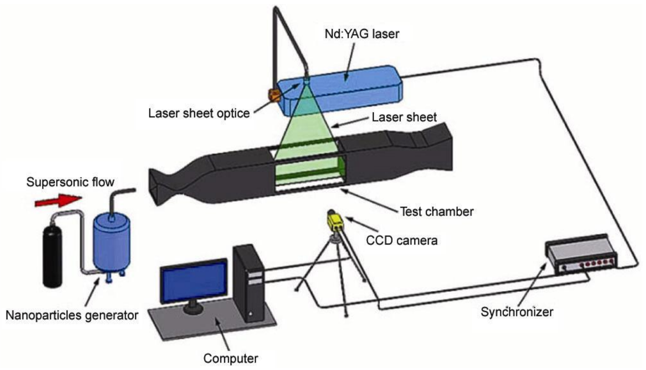

Figure 2. Nano-tracer-based planar laser scattering testing system.

Figure 3 *a* shows the NPLS image of instantaneous flow field, which distinctly reveals the fine structure and evolution. The origin of the coordinate axis is located at the corner. It can be seen from the figure that light scattered from the main flow region is homogeneous. However, light scattered from the boundary layer and separation region is weak because of fewer nanoparticles. The upstream turbulent boundary layer which is fully developed represents structural irregularities and intense fluctuations in the whole flow field. Flow separation occurs somewhere upstream of the ramp as a result of adverse pressure gradient and separation shock is formed. This is in agreement with the experimental results of Ringuette and Smits[14] and Bookey *et al.*[15] under the same conditions. Supersonic flow decelerates while its density increases because of the separation shock, which corresponds to the grey-level variations. Reattachment occurs somewhere on the ramp generating a recirculation zone between the separation point and the reattachment point, and a sheer

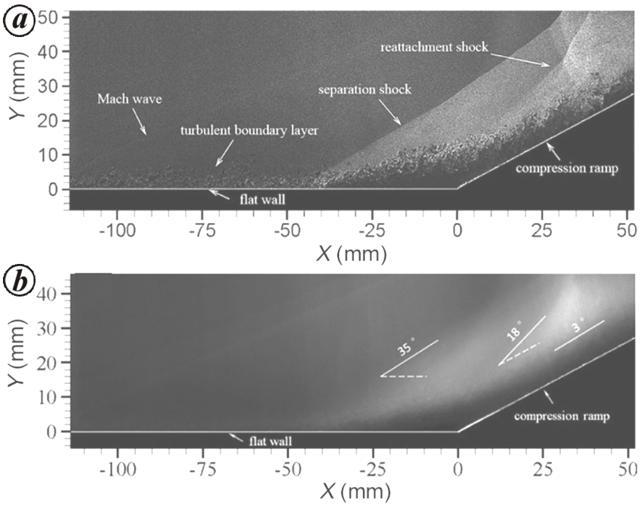

Figure 3. Flow structures of compression ramp: ***a***, instantaneous flow field and ***b***, time-averaged flow field.

layer is formed between the separated flow and the reverse flow region. Similar flow structures have been observed in the experiments conducted by Verma[16].

A time-averaged flow field can be obtained by performing an averaging process to hundreds of NPLS images (Figure 3 *b*). The time-averaged flow field is based on 400 instantaneous flow fields. Although transient characteristics are erased in the averaging process, flow unsteadiness are also eliminated, which is advantageous to analyse the time-averaged structural properties. It can be seen from the figure that the thickness of upstream turbulent boundary layer is about 6 mm, and the redeveloped boundary layer after reattachment is obviously thicker. Structures such as boundary layer, separation shock and reattachment shock can be identified by the image grey-level analysis and Canny edge detection technique[17]. Measurements show that the angle between the separation shock and the forepart flat is 35°, which is close to the shock angle (39°) measured by Verma *et al.*[18] in a Mach 2.0 compression ramp flow. The angle between the reattachment shock and the ramp is 18° and the turbulent boundary layer after reattachment increases at an angle of 3°.

Temporal evolution of flow field is shown in Figure 4, in which the time interval is 10 μs. Three typical large-scale structures are selected and compared. Structure 'A' at t_0 develops to become 'a' after 10 μs, it moves downstream about 6.2 mm and does not show obvious deformation which reveals that the characteristics of coherent structures in supersonic turbulent boundary layer are high speed and slow distortion. Structures 'B' and 'C' which are located at the external region of separated flow are affected by separation shock. Compared to 'b' and 'c' their velocity decreases significantly and they move downstream about 5.0 mm in the 10 μs interval. At the same time, 'b' and 'c' have showed obvious deformation as a result of the effects from the adverse pressure gradient and the reversed flow in separation region.

The flow field is divided into anterior and posterior regions for further analysis. Fine flow structures of local regions are shown in Figure 5. As shown in Figure 5 *a*, the thickness of turbulent boundary layer does not increase monotonously. While it changes constantly along the flow direction, there is a distinct feature that the distribution of the boundary layer is zigzag. This characteristic also illustrates the structural irregularities and intense fluctuations of turbulent boundary layer. The separation region which is formed by separated flow can be clearly seen from Figure 5 *b*. Some large-scale structures can be found in the incoming boundary layer, but they are not found in reattachment region and downstream regions. This may be due to three-dimensional effect and fracture of vortices caused by the separation shock and reattachment shock.

Figure 6 *a* and *b* shows the mean velocity field of the separation region. Flow separation occurs under the effects of adverse pressure gradient, and separation shock is formed. Being affected by separation shock, air flow decelerates and changes its direction to be parallel with the ramp. Separation and reattachment are revealed distinctly by streamlines; a recirculation zone including reverse flow and shear flow is created by separation, in which large velocity gradients are induced by intense shearing effects. Low-speed reverse flow exists in the region covered by shear layer; velocity distribution in main stream is homogeneous. Figure 6 *c* and *d* shows mean velocity distribution of separation region in streamwise (U) and vertical (V) direction. The main characteristics of the U component velocity are intense velocity shear and gradient variation; three-layered structures including main stream area, shear layer and recirculation zone are significant. It is interesting that the V-component velocity

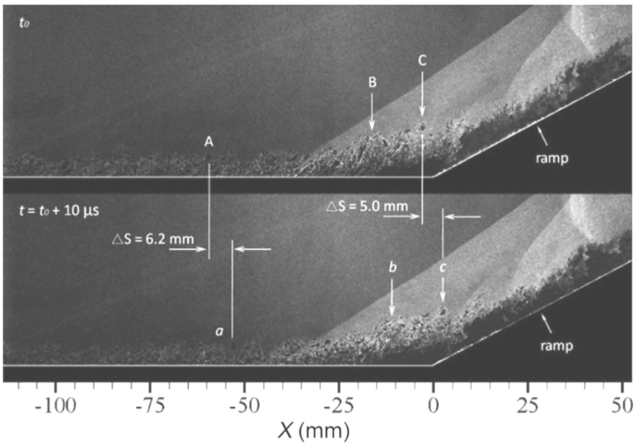

Figure 4. Time-evolution of flow field.

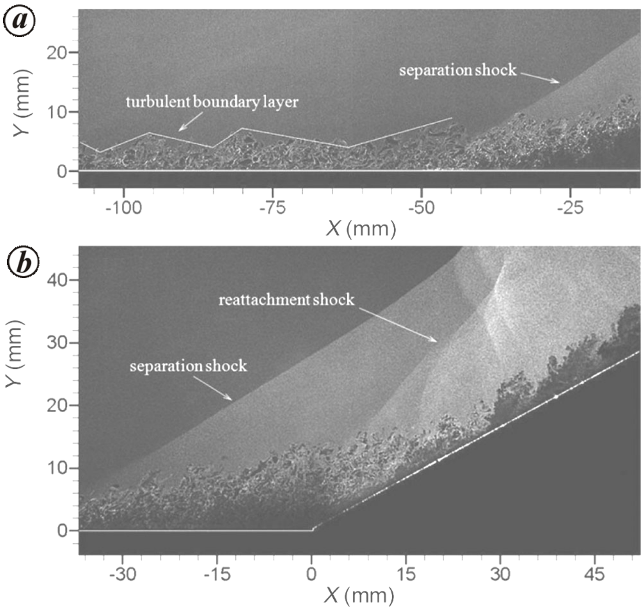

Figure 5. Flow structures in local regions: ***a***, Anterior region and ***b***, posterior region.

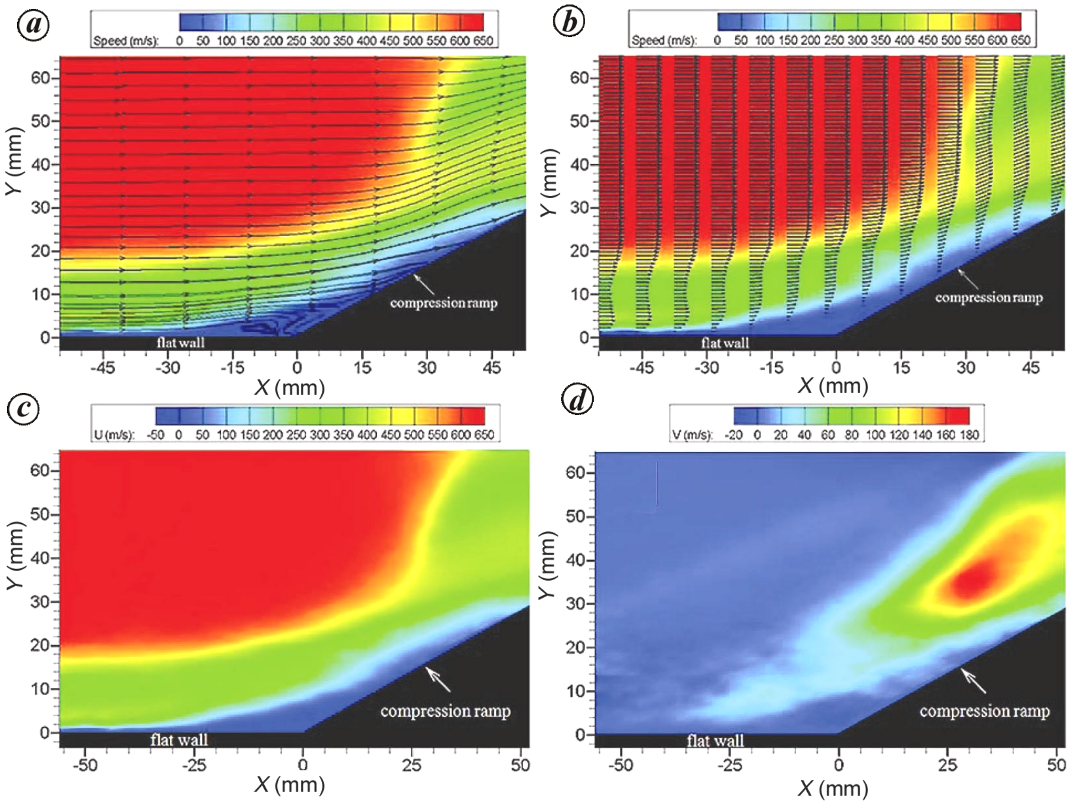

Figure 6. Velocity field structures of separation region. ***a***, streamline chart; ***b***, vector chart; ***c***, distribution of streamwise velocity; ***d***, distribution of vertical velocity.

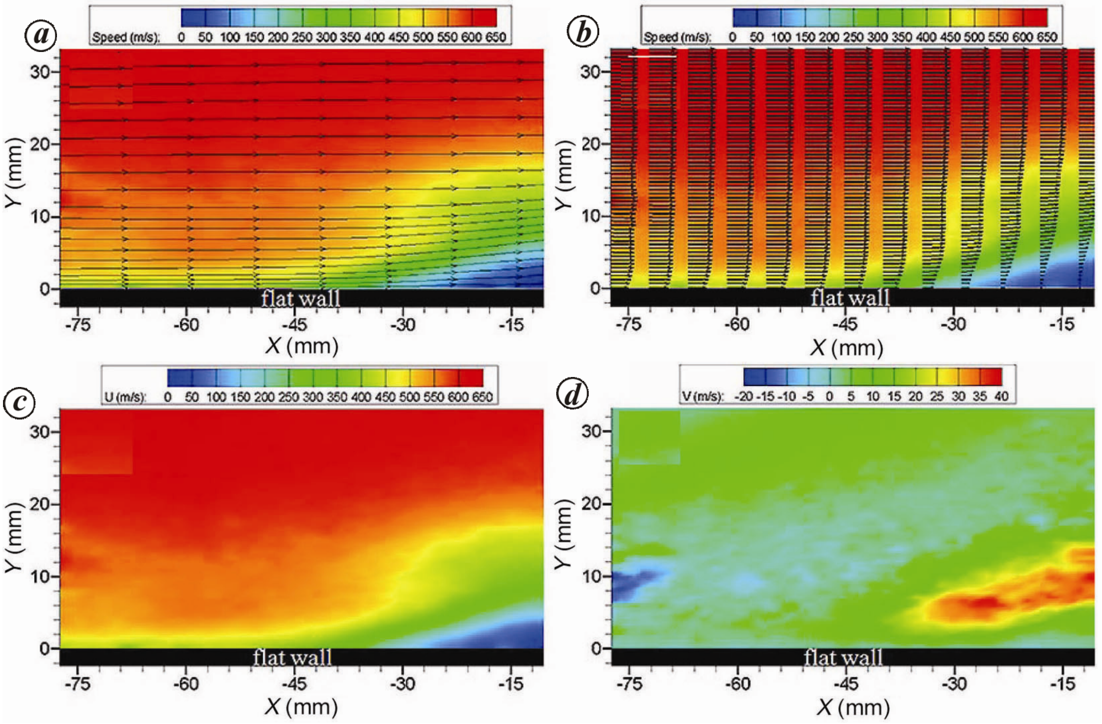

Figure 7. Velocity field structures in the vicinity of the separation point. ***a***, Streamline chart; ***b***, vector chart; ***c***, distribution of streamwise velocity; ***d***, distribution of vertical velocity.

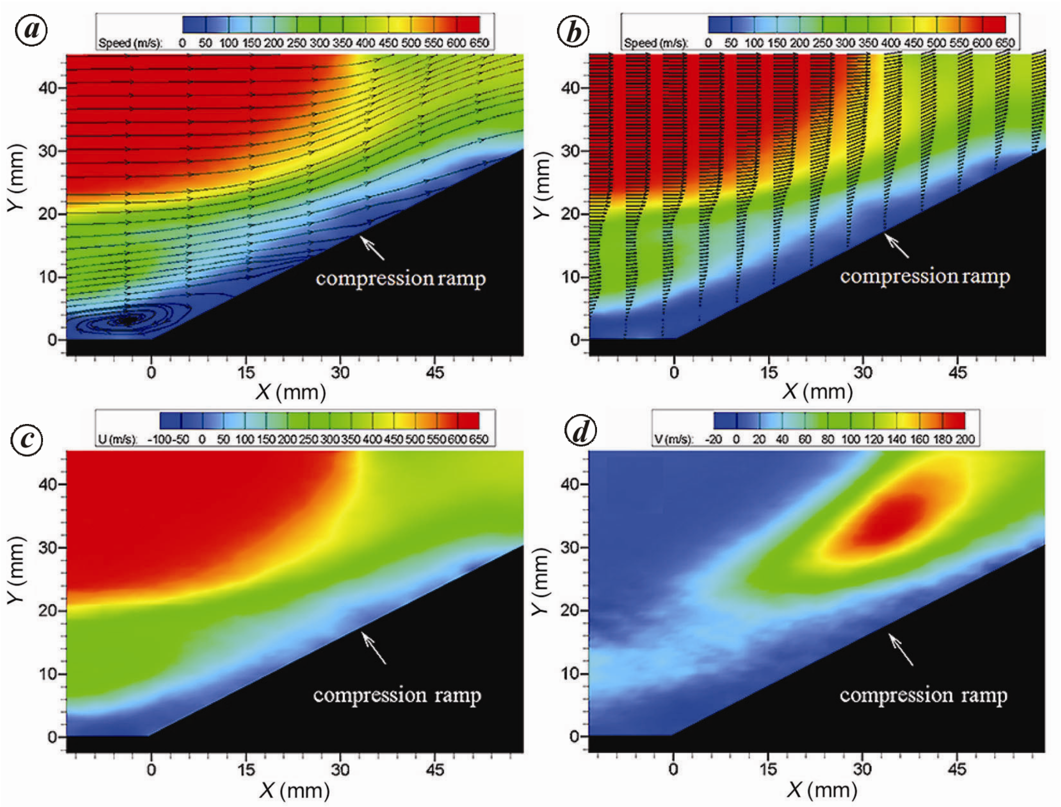

Figure 8. Velocity field structures in the vicinity of reattachment point. ***a***, Streamline chart; ***b***, vector chart; ***c***, distribution of streamwise velocity; ***d***, distribution of vertical velocity.

distribution is like an oblique *V*. From the bottom up along the *V*-direction, there is a recirculation zone near the ramp, where the velocity is much lower than that in the shear layer. As a result, the lower boundary of the oblique *V* is formed. Due to flow channel contraction, there is acceleration along the *V*-direction in main stream, and a local region where the *V*-component velocity is highest appears. Afterwards, the *V*-component velocity decreases gradually, the upper boundary of the oblique *V* which is composed of disturbance area and shock is formed.

Figure 7 *a* and *b* shows the mean velocity field in the vicinity of the separation point. Velocity profiles of upstream turbulent boundary layer are full; large velocity gradients exist along the normal direction, which is the typical characteristic of turbulent boundary layer. It can be concluded from the velocity chart that speed in the main stream area is about 620 m/s, while inside the boundary layer it increases rapidly from low speed to hundreds of metres per second along the normal direction. The influence of the adverse pressure gradient transmits upstream through the subsonic layer in the boundary layer. As a result, flow direction deflects from the location of *X* = –30 mm, and velocity profiles gradually become not full. The cloud chart shows that shear layer appears at the same position, where velocity profiles of shear layer begin to form. It can be inferred that flow separation occurs at the location *X* = –30 mm. Figure 7 *c* and *d* provides mean velocity distribution in streamwise (*U*) and vertical (*V*) direction of the same region. There are irregular variations in the *U*-component velocity of upstream turbulent boundary layer, which illustrates the structural irregularities and intense fluctuations again. Gradient variations do not exist in the *V*-component velocity, while fluctuations appear. The *U*-component velocity decreases distinctly from the location *X* = –30 mm and layered structures appear along the normal direction. At the same time, positive accelerations in the *V*-component velocity emerge from the same position. These changes indicate that the separation point is located at *X* = –30 mm.

Figure 8 *a* and *b* shows the mean velocity field in the vicinity of the reattachment point. The reverse flow and reattachment are well revealed by streamlines. The range of recirculation zone diminishes gradually, but the velocity gradients are still large. Reattachment point is located at the end of the recirculation region, boundary layer redevelops after reattachment, and the velocity gradients increase along the normal direction. Also the velocity profile gradually become full. With a comprehensive analysis of the streamlines and vector variations, it can be concluded that flow reattachment occurs at the location

$X = 25$ mm on the ramp, where the mean flow speed nearby the wall is zero. Figure 8 *c* and *d* shows the mean velocity distributions in the *U* (left) and *V* (right) components of the same region. It can be seen from the *U*-component velocity cloud chart that shear layer is gradually close to the ramp, and the recirculation region which is covered by shear layer decreases gradually. The distributions of the *V*-component velocity are a continuation of the oblique *V* in the separation region.

---

1. Wu MinWei and Martin, P. M., Analysis of shock motion in shock wave and turbulent boundary layer interaction using direct numerical simulation data. *J. Fluid Mech.*, 2008, **594**, 71–83.
2. Edwards, J. R. and Boles, J. A., Large eddy Reynolds-averaged Navier–Stokes simulation of a Mach 5 compression–corner interaction. *AIAA J.*, 2008, **46**, 977–991.
3. Dawson, D. M., Kawai, S. and Lele, S. K., Large-eddy simulation of a Mach 2.9 turbulent boundary layer over a 24° compression ramp. In 41st AIAA Fluid Dynamics Conference, Honolulu, Hawaii, AIAA 2011–3431, 27–30 June 2011.
4. Gramann, R. A. and Dolling, D. S., A preliminary study of the turbulent structures associated with unsteady separation shock motion in a Mach 5 compression ramp interaction. AIAA paper 1992–0744.
5. Ringuette, M. J., Bookey, P. and Wyckham, C., Experimental study of a Mach 3 compression ramp interaction at $Re_\theta = 2400$. *AIAA J.*, 2009, **47**, 373–385.
6. Chan, S. C., Clemens, N. T. and Dolling, D. S., Flowfield imaging of unsteady, separated compression ramp interaction. In 26th AIAA Fluid Dynamics Conference, San Diego, USA, AIAA 1995–2195, 19–22 June 1995.
7. Zheltovodov, A. A., Some advances in research of shock wave turbulent boundary layer interactions. In 44th AIAA Aerospace Sciences Meeting, Reno Nevada, AIAA 2006–0496, 9–12 January 2006.
8. Yi, S. H., He, L., Zhao, Y. X. and Tian, L. F., A flow control study of a supersonic mixing layer via NPLS. *Sci. China Ser. G-Phys. Mech. Astron.*, 2009, **52**, 2001–2006.
9. Zhao, Y. X., Yi, S. H. and Tian, L. F., Supersonic flow imaging via nanoparticles. *Sci. China Ser. E-Tech. Sci.*, 2009, **52**, 3640–3648.
10. He, L., Yi, S. H., Zhao, Y. X., Tian, L. F. and Chen, Z., Visualization of coherent structures in a supersonic flat-plate boundary layer. *Chin. Sci. Bull.*, 2011, **56**, 489–494.
11. Chen, Z., Yi, S. H., He, L., Tian, L. F. and Zhu, Y. Z., An experimental study on fine structures of supersonic laminar/turbulent flow over a backward-facing step based on NPLS. *Chin. Sci. Bull.*, 2012, **57**, 584–590.
12. Wu, Y., Yi, S. H., Chen, Z., Zhang, Q. H. and Gang, D. D., Experimental investigations on structures of supersonic laminar/turbulent flow over a compression ramp. *Acta Phys. Sin.*, 2013, **62**, 184702.
13. Zhu, Y. Z., Yi, S. H., He, L. and Tian, L. F., Instantaneous and time-averaged flow structures around a blunt double-cone with or without supersonic film cooling visualized via nano-tracer planar laser scattering. *Chin. Phys. B*, 2013, **22**, 014702.
14. Ringuette, M. J. and Smits, A. J., Wall-pressure measurements in a Mach 3 shock wave turbulent boundary layer interaction at a DNS-accessible Reynolds number. In 37th AIAA Fluid Dynamics Conference, Miami, FL, AIAA 2007–4113, 25–28 June 2007.
15. Bookey, P., Wyckham, C. and Smits, A. J., Experimental investigations of Mach 3 shock-wave turbulent boundary layer interactions. In 35th AIAA Fluid Dynamics Conference, Toronto, Ontario, Canada, AIAA 2005–4899, 6–9 June 2005.
16. Verma, S. B., Experimental study of flow unsteadiness in a Mach 9 compression ramp interaction using a laser schlieren system. *Meas. Sci. Technol.*, 2003, **14**, 989–997.
17. Zhao, Y. X., Yi, S. H. and He, L., The experimental study of interaction between shock wave and turbulence. *Chin. Sci. Bull.*, 2007, **52**, 1297–1301.
18. Verma, S. B., Manisankar, C. and Raju, C., Control of shock unsteadiness in shock boundary-layer interaction on a compression corner using mechanical vortex generators. *Shock Waves*, 2012, **22**, 327–339.

ACKNOWLEDGEMENT. This research is supported by the National Natural Science Foundation of China (Grant No. 11172326 and Grant No. 11302256).

Received 25 March 2014; revised accepted 23 September 2014

Prevalence of *Wheat dwarf India virus* in wheat in India

Jitendra Kumar[#], Jitesh Kumar[#], Shashank Singh, Vishnu Shukla, Sudhir P. Singh and Rakesh Tuli*

National Agri-Food Biotechnology Institute, Mohali 160 071, India

***Wheat dwarf India virus* (*WDIV*) is the first mastrevirus reported to have subgenomic molecules called satellites. To establish association of the satellites with *WDIV* across a variety of ecoclimatic conditions, a countrywide survey was carried out. *WDIV* and its associated satellites (alphasatellite and betasatellite) were identified in plant samples collected from each of the 14 field locations surveyed in the study. Though there were location- and variety-related differences in disease scale, most of the infected wheat cultivars in fields across the country carried both the satellites. The wide occurrence of *WDIV* disease complex in India suggests the need to assess how the spread of *WDIV* and its satellites can be limited in wheat fields.**

Keywords: Alphasatellite, atypical mastrevirus, betasatellite, symptom severity.

WHEAT *dwarf India virus* (*WDIV*) is a leafhopper (*Psammotettix* sp.; family Cicadellidae) transmitted mastrevirus (family Geminiviridae) that infects wheat in India[1]. Dwarfing or stunting is the typical symptom of *WDIV*, but yellowing of leaves is also associated with field infection, which may be due to other factors[2]. Two alphasatellites (Cotton leaf curl Multan alphasatellite and Guar leaf

---

*For correspondence. (e-mail: rakeshtuli@hotmail.com)

[#]Contributed equally to this work.